RESEARCH ARTICLE

Zika virus dysregulates human Sertoli cell proteins involved in spermatogenesis with little effect on tight junctions

Mahamud-ur Rashid[1,2]**, Ali Zahedi-Amiri**[1,2]**, Kathleen K. M. Glover**[1,2]**, Ang Gao**[2]**, Michaela E. Nickol**[1]**, Jason Kindrachuk**[1]**, John A. Wilkins**[2,3]**, Kevin M. Coombs**[1,2,4]*

1 University of Manitoba, Department of Medical Microbiology and Infectious Diseases, Winnipeg, Manitoba, Canada, **2** Manitoba Centre for Proteomics & Systems Biology, Winnipeg, Manitoba, Canada, **3** University of Manitoba, Department of Internal Medicine, Health Sciences Centre, Winnipeg, Manitoba, Canada, **4** Children's Hospital Research Institute of Manitoba, John Buhler Research Centre, Winnipeg, Manitoba, Canada

* kevin.coombs@umanitoba.ca

Abstract

Zika virus (ZIKV), a neglected tropical disease until its re-emergence in 2007, causes microcephaly in infants and Guillain-Barré syndrome in adults. Its re-emergence and spread to more than 80 countries led the World Health Organization in 2016 to declare a Public Health Emergency. ZIKV is mainly transmitted by mosquitos, but can persist in infected human male semen for prolonged periods and may be sexually transmitted. Testicular Sertoli cells support ZIKV replication and may be a reservoir for persistent ZIKV infection. Electrical impedance analyses indicated ZIKV infection rapidly disrupted Vero cell monolayers but had little effect upon human Sertoli cells (HSerC). We determined ZIKV-induced proteomic changes in HSerC using an aptamer-based multiplexed technique (SOMAscan) targeting >1300 human proteins. ZIKV infection caused differential expression of 299 proteins during three different time points, including 5 days after infection. Dysregulated proteins are involved in different bio-functions, including cell death and survival, cell cycle, maintenance of cellular function, cell signaling, cellular assembly, morphology, movement, molecular transport, and immune response. Many signaling pathways important for maintenance of HSerC function and spermatogenesis were highly dysregulated. These included IL-6, IGF1, EGF, NF-κB, PPAR, ERK/MAPK, and growth hormone signaling. Down-regulation of the PPAR signaling pathway might impact cellular energy supplies. Upstream molecule analysis also indicated microRNAs involved in germ cell development were downregulated by infection. Overall, this study leads to a better understanding of Sertoli cellular mechanisms used by ZIKV during persistent infection and possible ZIKV impacts on spermatogenesis.

Author summary

Zika virus has gained new significance during the past few years when it became associated with increased numbers of birth defects. Zika virus is primarily transmitted by

mosquitoes. However, it is becoming increasingly clear that there are other ways the virus can be transmitted. One of these ways is through sexual transmission. In order to better understand how Zika virus can persist in humans and may be transmitted sexually, we examined the interactions between Zika virus and Sertoli cells, a specialized male testicular cell responsible for sperm production. We examined how Zika virus infection affected more than 1300 Sertoli cell proteins and found that virus infection altered cellular pathways responsible for sperm production. At the same time, Zika virus had little effect upon overall structure of the cells. This information helps better explain the long-lived persistence of Zika virus in human male reproductive cells and the virus' capacity to be sexually transmitted.

Introduction

Zika virus (ZIKV) is considered a neglected tropical disease. It is a small enveloped arthropod-borne human pathogen (arbovirus) with a small positive-sense single-stranded RNA genome. ZIKV belongs to the family *Flaviviridae*, which includes other human pathogens such as West Nile virus (WNV), Dengue virus (DENV), Yellow fever virus (YFV), and Japanese encephalitis virus (JEV) [1]. ZIKV was discovered in 1947 in a sentinel monkey [2], and first isolated from humans in 1952 [3].

Followed by a few sporadic infections in Pakistan and Malaysia reported in 1977, ZIKV re-emerged in the Pacific islands in 2007 and spread to more than 80 countries/territories worldwide including regions in Latin America, USA, and Southeast Asia [4–6]. In February 2016, the World Health Organization (WHO) declared ZIKV a Global Health Emergency [7]. Because of the non-specific nature of ZIKV disease symptoms and that >80% of patients remain asymptomatic, the virus was neglected for a long time [8]. The virus received recent major attention due to its association with Guillain-Barré syndrome in adults and microcephaly in newborns [3, 4, 8].

ZIKV is mostly transmitted by *Aedes* mosquitoes (*A. aegypti* and *A. albopictus*) in endemic areas [9], but sexual transmission was suggested from traveler-associated infections in non-endemic countries/territories [7, 10–12]. ZIKV can persist in infected male semen for prolonged periods in the absence of viremia and disease symptoms. Live ZIKV and viral RNA were detected in semen up to 370 days after disease onset [13–15]. ZIKV infection causes severe pathological effects in male murine testicular tissues and reduces sperm motility and fertility [16, 17]. *In vitro* studies demonstrated that ZIKV can infect human testicular tissue and replicate in human Sertoli cells (HSerC), which may be a reservoir for long-term viral persistence [16, 18, 19].

Sertoli cells are considered the "mother" for spermatogonial stem cells, as they play critical roles in testis formation and aid the spermatogenesis process by supplying nutrients and developmental signals [20]. They also provide structural support to germ cells and create the blood-testis barrier (BTB) to ensure an immune-privileged environment to protect sperm cells from immune attack [21]. Unlike other bodily cells, HSerC depend upon fatty acid (FA) oxidation rather than glucose for energy [22]. The Peroxisome Proliferator-Activated Receptor (PPAR) signaling pathway plays an important role in energy generation by lactate and lipid oxidization [23]. Sertoli cells can influence the regulation of hormones, growth factors, and receptor signaling important for spermatogenesis and human fertility [24]. Follicle-stimulating hormone (FSH) is one of the key endocrine hormones that directly regulates spermatogenesis [25]. Sertoli cells secrete inhibin B after induction by FSH [26], but the level of inhibin B also provides

negative feedback on FSH secretion [27]. The level of serum inhibin B directly correlates with sperm count and is used as a marker for spermatogenesis [27].

In vitro and *in vivo* studies demonstrated that ZIKV persists in Sertoli cells [16, 18], but the mechanism(s) underlining persistence is/are unknown. Although Sertoli cells play many critical roles in germ cell development, the impact of ZIKV infection on the spermatogenesis process is not well understood. In this study, we determined the impact of ZIKV infection on proteins known to be important for HSerC function and spermatogenesis.

We used Slow Off-rate Modified Aptamers (SOMAmers; SomaLogics, Inc., Denver, CO), a multiplexed proteomic technique that measures 1305 unique proteins in up to 88 different samples simultaneously with high precision [28], and found that numerous proteins involved in multiple bio-functions were dysregulated. Bioinformatic analyses predict that many of these proteins, and upstream regulatory elements, are involved in germ cell development and spermatogenesis, which has important implications for male fertility and reproduction.

Results

ZIKV infectivity and cytopathic impact on primary HSerC

Primary HSerC were infected with ZIKV at MOI = 3, then virus infectivity and impact on cells were monitored up to 9 days post-infection (dpi). There was no observable ZIKV-induced cytopathic effect (CPE) throughout the tested infection course (Fig 1A). Cell viabilities declined to approximately 80% on days 5, 7 and 9 but were not statistically different from non-infected mocks (Fig 1B). Supernatant virus titers were determined by plaque assay. The number of progeny viruses started rising by 1 dpi, reached a peak of 4.4×10^6 PFU/ml by 5 dpi, but dropped below 10^5 PFU/ml by 7 and 9 dpi (Fig 1C). The rise in viral titer also corresponded with increased appearance of viral non-structural protein 1 (NS-1; Fig 1D), a marker of productive infection.

The lack of apparent ZIKV-induced HSerC CPE even after 9 days, and the function of HSerC to form the BTB led us to more quantitatively assess the impact of virus infection on cellular barrier function. We used electric cell-substrate impedance sensing (ECIS) to obtain real-time measurements of impedance and of CPE. We also used Vero cells, which, although they do not normally form tight-junction barriers, are highly susceptible to ZIKV and experience rapid CPE. The Vero cells experienced a total loss of electrical resistance by 75 hpi when infected at MOI 0.3, and lost resistance sooner at a higher MOI of 3 (Fig 2A). Disruption was also observed microscopically (Fig 2C). Conversely, HSerC infection with ZIKV at MOI 0.3 resulted in no changes in resistance during the first 47 h of infection, and only a small loss in resistance at 51 hpi (75h post-plating), which mimicked the trend seen in mock-infected cells (Fig 2B). HSerC infected with ZIKV at higher MOI of 3.0 showed no loss in resistance until 40 hpi (64h post-plating) and only moderate loss of resistance later, confirming that ZIKV infection of HSerC has only moderate effects on cell barrier integrity, which also was reflected by considerably lower CPE (Fig 2D). Based on these collective observations, we selected day 1 (early), day 3 (mid) and day 5 (peak virus titer) for subsequent global proteomic screens.

Proteomic dysregulation in HSerC after ZIKV infection

We used SOMAscan, a multi-plexed targeted system that can detect 1305 proteins simultaneously from each of up to 88 samples, to examine ZIKV infection-induced HSerC proteomic dysregulation. Samples were collected at 1, 3, and 5 dpi and time-matched non-infected mock samples, from each of three biological replicates. P values were determined by T-test and Z-scores, as detailed in Materials and Methods. A total of 358 proteins were deemed significantly dysregulated at any time point (Table 1). Almost 300 proteins were significantly dysregulated
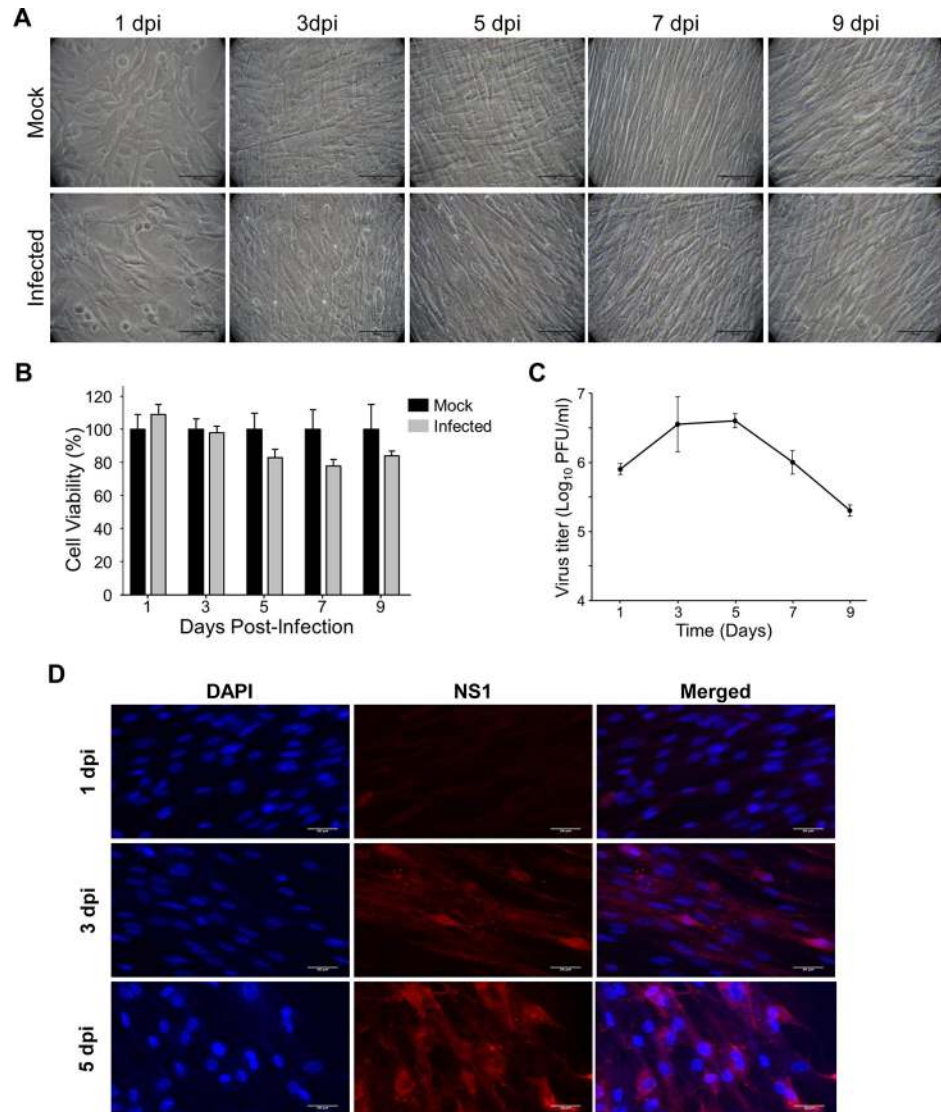
Fig 1. Zika virus (ZIKV) infectivity and cytopathic impact on human primary Sertoli cells (HSerC). HSerC were infected with ZIKV at an MOI of 3. Cell morphology, cell viability, and virus titer were measured every alternate day from day 1 to 9. (A) Cells were visualized under bright-field microscopy at 200× magnification and assessed for cytopathic effect. Scale bar is 50 μm. (B) HSerC viability was measured after ZIKV infection by WST-1 assay. (C) Virus titer in the infected cell supernatant was determined by plaque assay. The experiment was done in three replicates. (D) HSerCs were fixed after Day 1, 3 and 5 days post ZIKV infection, and viral protein expression was determined by fluorescent microscopy using ZIKV-NS1 monoclonal antibodies. Images were taken at 200× magnification. Scale bar is 20 μm. Cell nuclei were visualized by DAPI stain. dpi = days post-infection.

more than 1.3-fold, and more than 125 proteins were significantly dysregulated more than 2-fold. Irrespective of whichever fold-change cut-offs we choose, we generally found that most dysregulated proteins were downregulated at 3 dpi, whereas most were upregulated at 5 dpi (Table 1; Fig 3A and 3B). For subsequent bioinformatics analyses we considered fold-change cut-offs of ± 1.3-fold and fold-change cut-offs of ± 1.5-fold, both with $p < 0.05$, compared to mock. Apart from differences in numbers of significantly considered proteins at these two cut-off levels, there were no major changes in identified pathways, networks and bio-functions; thus, for more completeness, we consider significant cut-offs of ± 1.3-fold below. Collectively,
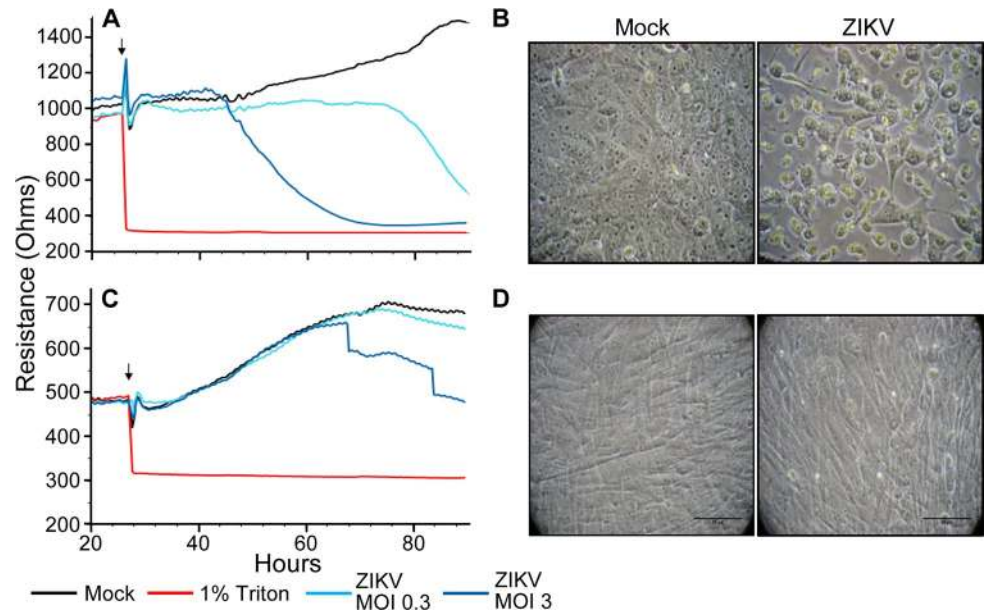
Fig 2. Electrical impedance of ZIKV-infected Vero (A) and HSerC (C). Cells were added to 96-well ECIS plates and allowed to grow for 24h to create monolayers. Cells were then treated, at time indicated with small vertical arrows, with media alone (positive control; black line), 1% Triton X-100 (negative control; red), or with ZIKV at MOI of 0.3 (teal) or 3.0 (dark blue) and cultures maintained with continuous impedance monitoring for another 66–80 hours. Values represent the averages obtained from 8 wells for each condition, and HSerC were analyzed twice. Micrographs of Vero (**B**) and Sertoli (**D**) cells at 72 hpi demonstrating observable CPE.

https://doi.org/10.1371/journal.pntd.0008335.g002

299 proteins were significantly dysregulated at any of the three different time points, with 12 (9 up- and 3 down-regulated) dysregulated at 1 dpi, 95 (25 up- and 70 down-regulated) dysregulated at 3 dpi, and 218 (201 up- and 17 down-regulated) dysregulated at 5 dpi (Table 1, Fig 3A, S1 Table). Protein abundance heat maps and clustering analysis showed there were 14 significantly down-regulated proteins at day 3 dpi that were significantly up-regulated at 5 dpi, whereas 3 proteins were up-regulated at both time points (Fig 3B; Table 1; S1 Fig). We validated several proteins' dysregulation by Western blot, based on high fold-changes and

Table 1. Numbers of significantly dysregulated ZIKV-infected HSerC proteins.

Number that are significant	Total Unique	1 dpi	3 dpi	5 dpi
and Fold-change > 1.00	358	16	46	213
and Fold-change < -1.00		5	90	21
and Fold-change > 1.10	354	13	45	212
and Fold-change < -1.10		5	89	21
and Fold-change > 1.30	299	9	25	197
and Fold-change < -1.30		5	67	17
and Fold-change > 1.50	216	4	19	152
and Fold-change < -1.50		0	51	12
and Fold-change > 2.00	128	0	10	100
and Fold-change < -2.00		0	30	6
and Fold-change > 3.00	71	0	5	53
and Fold-change < -3.00		0	21	1

Significance was determined by T-test and Z-score ($p < 0.05$) as detailed in Methods

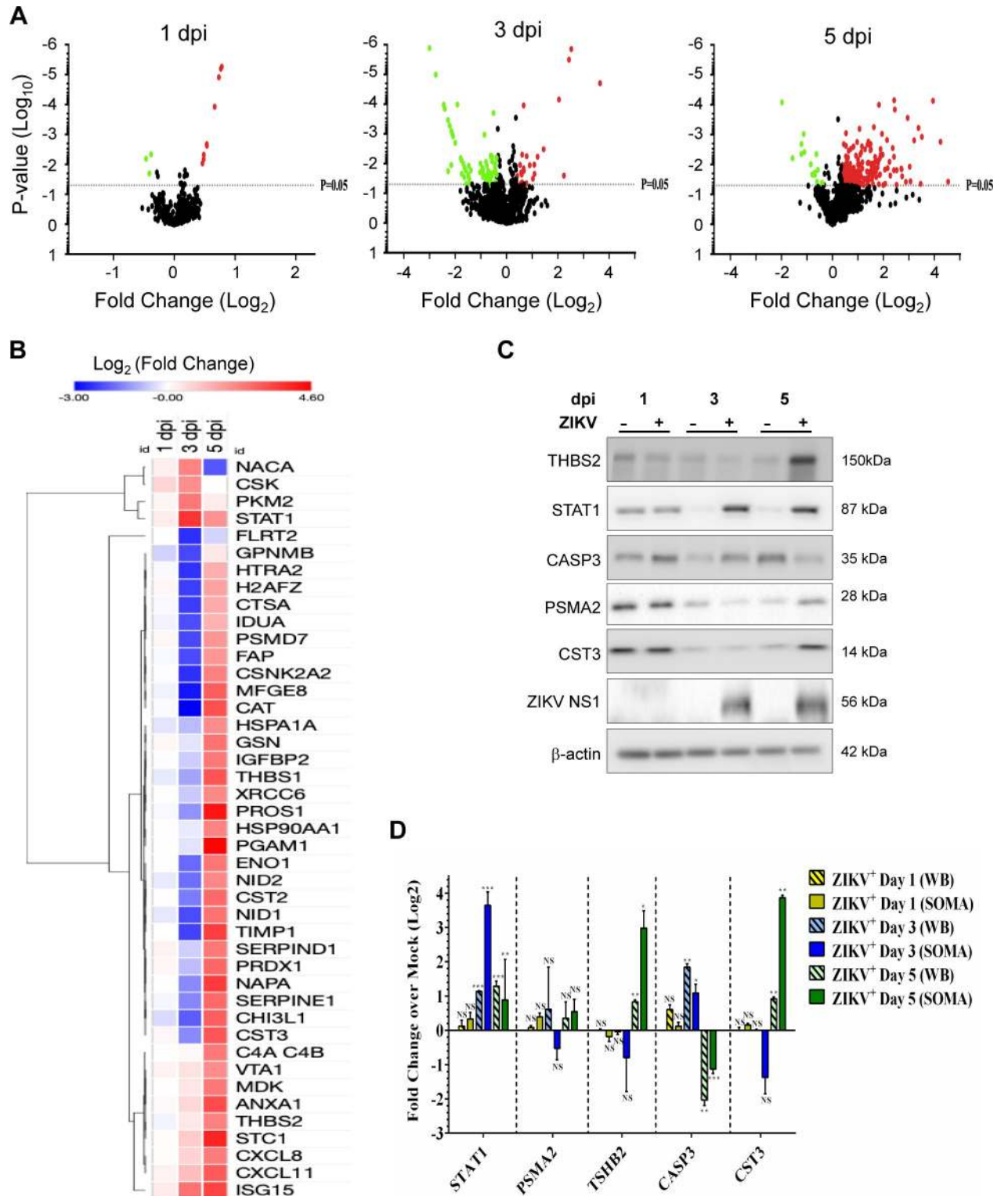https://doi.org/10.1371/journal.pntd.0008335.t001

Fig 3. Proteomic analyses of ZIKV-infected HSerC by SOMAscan. (**A**) Volcano plots showing the expression fold changes and the significance of differentially expressed proteins at 1, 3 and 5 dpi (P-value < 0.05). Up- and down-regulated proteins are highlighted in red and green, respectively. (**B**) Heat map of selected differentially expressed (fold change > 4 or < -4) proteins at 1, 3 and 5 days post ZIKV infection. Up- and down-regulated proteins are highlighted in red and blue, respectively. (**C**) Validation of SOMAscan results by Western blot of 5 selected differentially regulated proteins. (**D**) Expression value of the proteins from Western-blot were quantified from three replicates and plotted side-by-side to SOMAscan

antibody availability (Fig 3C) and confirmed similar patterns of expression (Fig 3D). For example, STAT1 was not significantly dysregulated by 1 dpi as measured by both SOMAscan and immunoblot, and, although absolute fold-change values differed between SOMAscan and immunoblot, both methods indicated STAT1 was significantly up-regulated by 3 and 5 dpi.

ZIKV dysregulates cellular functions and signaling pathways in HSerC

The list of significantly dysregulated proteins was uploaded into IPA to determine ZIKV-induced impacts on cellular protein networks, signaling pathways and cellular functions. IPA could not predict any networks with confidence at 1 dpi because of the low numbers of dysregulated molecules. A total of 11 networks were predicted by IPA at 3 dpi (n = 5) and at 5 dpi (n = 6) that had scores >20 and comprised 11 or more focus molecules (S2 Table, S2 Fig). Changes in protein expression as a function of progressing infection were constructed for three of these networks (Cell-to-cell signaling, Cell death and survival, and Post-translational modification; S3 Fig) and demonstrate little, if any dysregulation at 1 dpi, general down-regulation at 3 dpi and general activation at 5 dpi. Proteins expressed differentially after ZIKV infection at 3 dpi and 5 dpi were classified into three functional categories, including biological processes, cellular components, and molecular functions by GOTERM and PANTHER. A wide range of biological process subcategories were enriched at 3 dpi, with some of the highest enrichment scores from up-regulated proteins attributed to JAK-STAT cascade, chromatin assembly, and negative regulation of apoptotic process (S4 Fig). The vast majority of these biological processes were not enriched later at 5 dpi; instead up-regulated proteins at this later time showed higher enrichment for entirely different classes of biological processes, such as gluconeogenesis, angiogenesis, glycolysis, and protein phosphorylation. Similar differential biological process enrichment patterns also were observed for down-regulated proteins, and in molecular functions at 3 dpi compared to 5 dpi. Cellular growth and proliferation, post-translational modification, cellular development, and cell signaling were significantly decreased and immune cell trafficking, and cell death by apoptosis were significantly increased at 3 dpi (S3 Table).

Bio-function analysis by IPA also predicted that development of gap junctions, assembly of intercellular junctions and protein phosphorylation were significantly downregulated, whereas protein fragment hydrolysis and organismal death were increased (Fig 4A). At 5 dpi, cell death by necrosis, post-translational modification and protein synthesis were significantly decreased and cellular movement, immune cell trafficking, cell viability, cell-to-cell signaling, cell proliferation, cell cycle, cellular development and maintenance, cellular assembly and inflammatory response were significantly increased (Fig 4B, S4 Table).

Based on the dysregulated proteins, IPA predicted a total of 383 canonical pathways that were significantly affected by 5 dpi. Among them, the top 20 pathways are Il-6, IGF-1, HMGB1, IL-3, IL7, GM-CSF, Telomerase, EGF, NF-kB, PPAR, 14-3-3 mediated, VEGF, FGF, Thrombopoietin, IL-8, Renin-Angiotensin, ERK/MAPK, Integrin, Growth hormone, and JAK/Stat signaling pathways (Fig 4D). The PPAR pathway was the only significantly down-regulated pathway at this time point. HSP90AA1, HSP90AB1, IL1R1, ILRAP, IL36A, IL37, MAPK1, PTGS2, SHC1, and TNFRSF11B, all involved in PPAR pathway, were significantly up-regulated at 5dpi (Fig 4E). Direct and indirect IPA-predicted protein interactions suggest metal ion, synthesis of nitric oxide, and LDH levels will significantly decrease, but antigen presentation will increase in HSerC by 5dpi (Fig 4F). IPA predicted another 205 proteins that
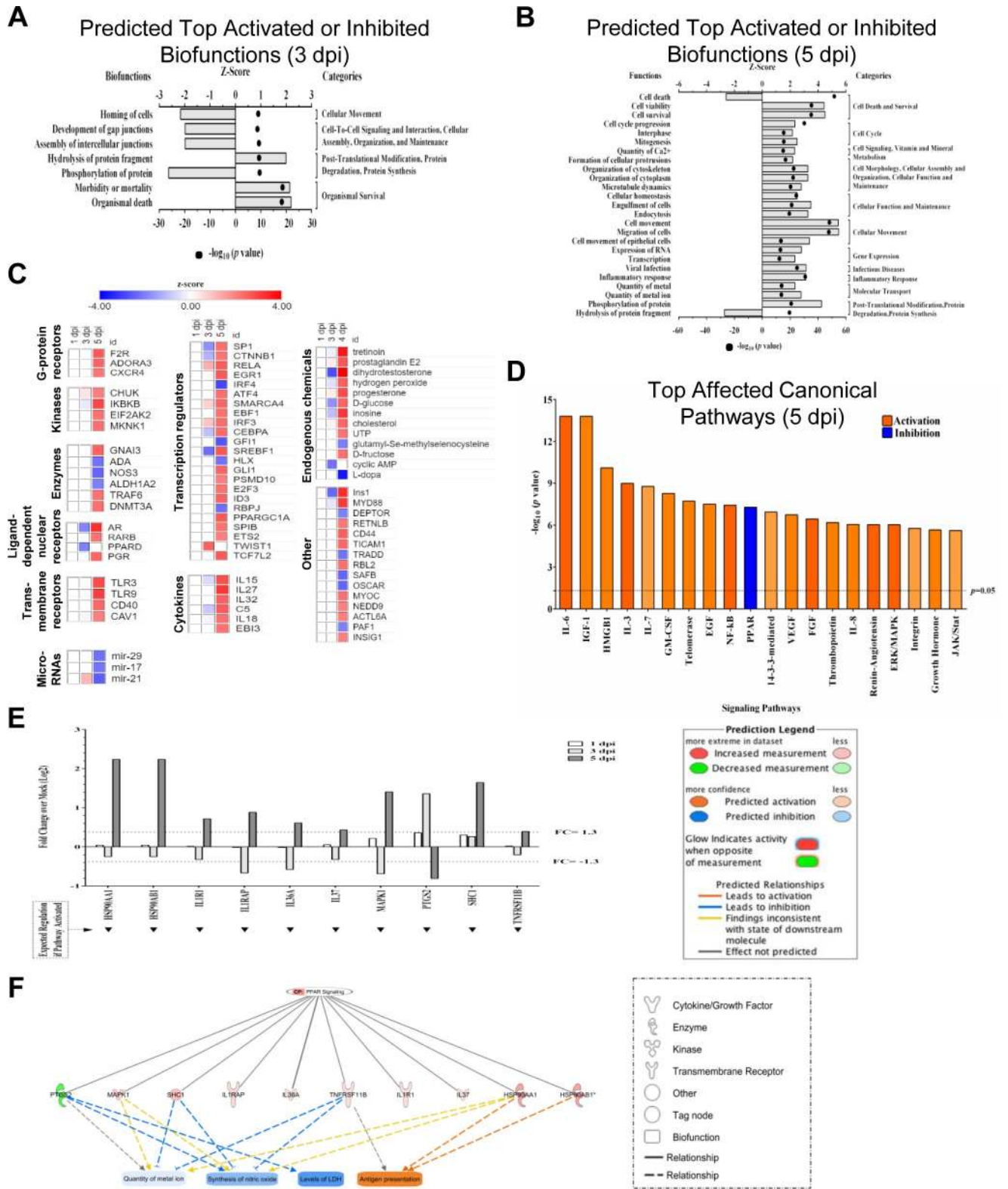
Fig 4. IPA-predicted activation and inhibition of bio-functions, upstream molecules, and canonical pathways. (A) Top bio-functions and predicted activation or inhibition Z-Scores (upper x-axis) and Log_{10} p-values (lower x-axis) are indicated at 3 dpi and (B) 5 dpi. Activation is indicated by positive Z-Score and the inhibited bio-functions are indicated by negative Z-scores. Major bio-function categories are indicated at right. (C) Top upstream molecules and prediction of their activation or inhibition based on Z-Scores. (D) Top affected canonical pathways with Log_{10} p-value indicated at the top.

Orange corresponds to activation, and blue corresponds to inhibition, with the degree of coloration corresponding to Z-Score. (E) ZIKV-induced inhibition of selected proteins within the PPAR signaling pathway as a function of time post-infection. Note that by 5 dpi, all proteins are dysregulated ≥ 1.3-fold. (F) Predicted effects of indicated PPAR pathway proteins on various bio-functions.

were up-regulated and 75 down-regulated by upstream analysis by 5 dpi. These proteins belong to G-protein receptor, kinases, enzymes, transmembrane receptors, transcription regulators, cytokines, microRNAs, and endogenous chemicals. Many of the predicted upstream molecules are involved in maintenance of HSerC function and spermatogenesis (Fig 4C).

Because of the large numbers of dysregulated proteins and pathways described earlier, we then focused on those proteins significantly dysregulated >5-fold. Of the 26 proteins that exceeded this threshold, 20 were dysregulated at 5dpi, 7 at 3 dpi, only 1 (ISG15) was dysregulated >5-fold at both time points, and no proteins were dysregulated >5-fold at 1dpi. The dysregulated proteins belong to cytokines (TIMP1, CXCL11, CXCL8), enzymes (ANXA1, CHI3L1, CHI3L1, CAT), growth factor (MDK), kinases (STC1, PKM), peptidase (HTRA2), phosphatase (PGAM1), transcription regulator (STAT1), transporter (NAPA), and others (S5 Fig). The five top-most dysregulated proteins are phosphoglycerate mutase 1 (PGAM1), protein S (PROS1), stanniocalcin 1(STC1), NSF attachment protein alpha (NAPA) and TIMP metallopeptidase inhibitor 1(TIMP1), with expression levels >11-fold compared to non-infected at 5dpi. Sixteen of the 26 top dysregulated proteins are predicted to affect cell-to-cell signaling and interaction, immunological disease, organismal injury and abnormalities in cellular networks.

ZIKV disrupts the expression of Inhibin B by HSerC

In light of the many dysregulated proteins being involved in maintenance of Sertoli cell function and spermatogenesis (Fig 4C) and to better delineate potential functional consequences of ZIKV infection on spermatogenesis, we determined inhibin B levels in culture supernatants after infection and follicular stimulating hormone (FSH) treatment. FSH concentrations of 62.5 and 125ng/ml caused 1.1- and 2.4-fold increases in inhibin B expression, respectively (Fig 5). However, ZIKV infection caused significant reductions in inhibin B expression.

Discussion

ZIKV is an arbovirus, transmitted by mosquitoes, but unlike other known members of the *Flaviviridae* family, can also be transmitted sexually [29–31]. Although sexual transmission is not the main mode of ZIKV transmission, patients may be infected this way in non-endemic areas. Long term ZIKV persistence in semen after disappearance of disease symptoms increases the chances of sexual transmission. *In vivo* studies demonstrate that ZIKV can replicate in murine [17, 32, 33], hamster [34] and macaque testes [35, 36]. The virus caused severe inflammation and tissue destruction in murine testes [17, 32, 33], but similar effects have not been observed in humans. ZIKV can replicate in HSerC, which likely support viral persistence [18, 37], but the mechanism underlying this is not well understood.

We explored the impact of ZIKV infection on the HSerC proteome to complement earlier ZIKV-induced transcriptomic studies [18]. Unlike murine Sertoli cells [38], HSerC support high levels of ZIKV replication without any notable CPE up to 9 dpi (Fig 1A), as observed in other studies [18, 37]. ZIKV induced more dysregulation of the cellular proteome over time. Most dysregulated proteins were downregulated at 3 dpi whereas more proteins were upregulated at 5 dpi. Notably, at least 4 of these proteins (CASP3, HTRA2, SERPINE1, and SNCA) are associated with cell death, which is predicted to be increased by 3 dpi but decreased by 5 dpi. Thus, initially during active virus replication, cells were pushed towards cell death but
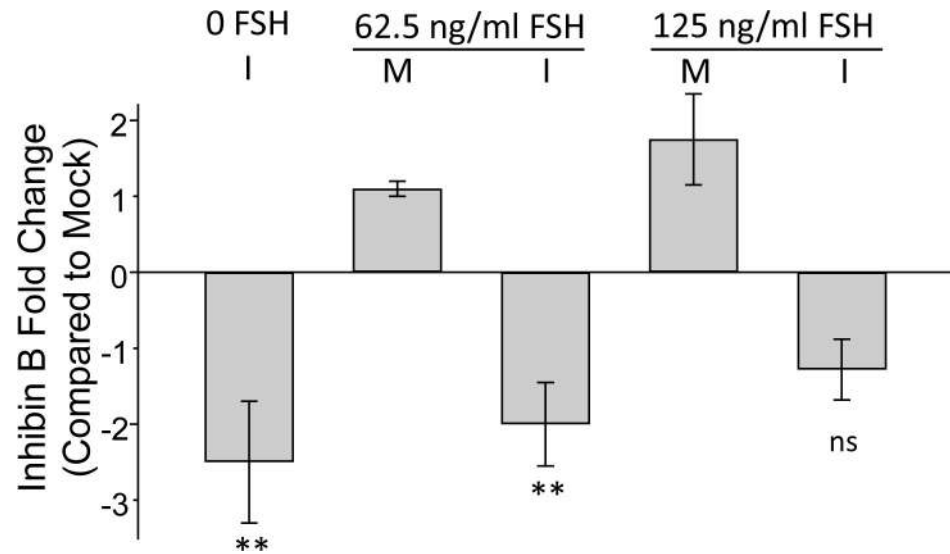
Fig 5. Inhibin B secretion by HSerC after FSH treatment and ZIKV infection. Cells were infected (I) with ZIKV at MOI = 3, or non-infected mock (M), and treated with indicated concentrations of follicular stimulating hormone (FSH) for 48 hours. Impact of infection and FSH on inhibin B production monitored by ELISA and compared to non-infected/non-treated controls. n = 3. ** = p-value < 0.01, * = p-value < 0.05.

https://doi.org/10.1371/journal.pntd.0008335.g005

later recovered, while virus titers started dropping after 5 dpi (Fig 1B and 1D). IPA also predicted similar observations based on the whole dataset analysis (S2 Table–S4 Table). These data are suggestive of a switch from an acute infection to a non-CPE persistent infection.

ZIKV disrupts proteins involved in HSerC functions related to spermatogenesis

A large number of proteins known to play critical roles in HSerC functions, including innate immunity and spermatogenesis, were dysregulated by ZIKV infection. Pyruvate kinase (PKM2), an important regulator of the glycolysis pathway, was elevated in ZIKV-infected HSerC at 3dpi. Phosphoglycerate mutase 1 (PGAM1), another important regulator of glycolysis, was the most dysregulated protein at 5dpi. PGAM1 is a critical enzyme that plays important roles in cell proliferation, migration, and apoptosis [39]. Elevated expression often is associated with cancer [40–42] and spermatogenic dysfunction [39, 43].

Metalloproteinase inhibitor 1 (TIMP1) is a glycoprotein inhibitor of Matrix Metalloproteinases (MMPs) [44] that was expressed >10-fold higher in ZIKV-infected HSerC compared to mock. MMPs and TIMPs participate in matrix remodeling, fibrosis, semen liquefaction [44–47] and regulate Sertoli cell-tight junction dynamics [48]. TIMP1 is an important regulator for both testicular development and spermatogenesis [49]. TIMP1 was highly expressed in ZIKV-infected endothelial cells [50], is intimately involved in maintaining fetal membrane integrity until labor [51], and amniotic fluid levels decrease during pregnancy with advancing gestation [52]. Coordinated regulation of MMPs and TIMPs are required to maintain tissue architecture and normal ovarian function [53, 54]. Thus, ZIKV-induced abnormal expression of TIMP1 may hinder spermatogenesis, the ovulation process, and may cause premature fetal delivery. Thus, the impact of ZIKV infection on ovarian development and premature fetal delivery also needs to be investigated. However, the impact of over expression of TIMP1 on the BTB is not well understood as it regulates collagen degradation by a negative feedback mechanism [48].

Vitamin K-dependent protein S (PROS1), Stanniocalcin-1 (STC1), and Alpha-soluble NSF attachment protein (NAPA) were also among the top 5 most dysregulated proteins in ZIKV-infected HSerC. PROS1 is an anticoagulant cofactor to activated protein C in blood coagulation regulation [55], involved in leukocyte migration, apoptosis, and activation of complement [56]. Over expression of PROS1 may cause inhibition of macrophage-mediated killing of ZIKV-infected cells and protect the cells from apoptotic death. Stanniocalcin-1 (STC1) is an estrogen-regulated gene expressed by Sertoli, Leydig and spermatogonias in rat testes [55, 57] and important for testis development [58, 59]. STC1 also is strongly linked with pregnancy complications [60]. NAPA is critical for the fertility of both male and female mice [61, 62]. Further study is necessary to better understand the roles of STC1 and NAPA in ZIKV pathogenesis.

The IL-6 signaling pathway was predicted as the most significantly upregulated at 5dpi. Overexpression of IL-6 adversely affects differentiation during spermatogenesis [63] and stimulates disruption of the BTB [64]. IGF1 receptors play crucial roles in maintenance of testis size and sperm production [65]. *In vivo* studies showed ZIKV reduces murine sperm count and testis size [17, 32, 33]. Human sperm counts were reduced after ZIKV infection [66] but the impact on testis size is unknown. The IGF-1 signaling pathway was predicted to be highly activated in HSerC by 5dpi. Granulocyte macrophage-colony stimulating factor (GM-CSF), a growth factor that stimulates porcine spermatogonia survival [67], was also highly activated by 5dpi. Blocking epidermal growth factor (EGF) receptors suppresses spermatogonial proliferation in newts [68].

Apoptotic cell death induced by controlled activation of nuclear factor-κB (NF-κB) signaling is needed to balance testicular germ cell production in healthy individuals [69]. NF-κB expression is also dependent on spermatogenesis stages [70]. Overactivation of NF-κB signaling induces excess sperm killing and causes infertility [71]. This pathway was highly activated at 5dpi and could explain low sperm counts in ZIKV-infected semen. Fibroblast growth factor (FGF) signaling, which was also highly activated by ZIKV infection, is an important pathway for regulating the male reproductive system [72] and maintenance of undifferentiated spermatogonia [73]. Fibroblast growth factors are hormones that stimulate DNA synthesis and proliferation of Sertoli cells [74], and overexpression can cause testicular tumors [75]. A transcriptomic study also confirmed that fibroblast growth factor-2 (FGF2) gene was highly expressed in ZIKV-infected Sertoli cells and might be associated with viral persistence [18]. ZIKV infection has not been found associated with testicular tumors in any study to date, but the long-term effects are unknown, which needs further investigation. Higher activation of mitogen-activated protein kinases (MAPKs) might also adversely impact the function of spermatozoa and spermatogenesis as regulated by the pathway [76].

Germ cell energy homeostasis is regulated through Sertoli cell function [77]. The PPAR pathway plays an important role in Sertoli energy generation. For example, activation of the pathway is required for lipid droplet formation, lactate production and metabolism [77, 78]. Downregulation of the PPAR pathway might dysregulate Sertoli energy supplies and adversely affect spermatogenesis. IPA also predicted downregulation of lactate-dehydrogenase (LDH) levels and quantity of metal ions (Fig 4C). Lactate and pyruvate are critical substrates for energy generation supplied by Sertoli cells to spermatocytes [79, 80].

MicroRNAs (miRs) also play critical roles in male fertility and spermatogenesis by controlling germ cell gene expression [81–83]. Self-renewal of murine germ cells is regulated by mir-21 [84]. The absence of *miR-17-92* cluster genes in Sertoli cells can change the testicular phenotype with an alteration in the whole transcriptome [85]. Upstream IPA analyses predicted *miR-17* and *mir*-21 were significantly downregulated in Sertoli cells by ZIKV infection, which might have an adverse impact on spermatogenesis and testes morphology.

ZIKV disrupts HSerC proteins involved in BTB tight junctions

Overactivation of the ERK/MAPK pathway disrupts the BTB, Sertoli–germ cell anchoring junction, and increases tight junction permeability [54, 86–88]. ERK pathway activation was also required for YFV replication [89]. ZIKV infection dysregulated the MAPK pathway in human neural progenitor cells [90] and in Sertoli cells by transcriptomic analysis [91]. The over activation of ERK/MAPK pathway indicates the possibility of BTB damage and disruption of this immune-privileged environment for the spermatogenesis process. The pathway might also be required for ZIKV replication, as observed in other members of the *Flaviviridae* [89, 92, 93]. Sertoli cell tight junctions are regulated by nitric oxide synthesis [94], and down regulation might impact BTB integrity. IPA also predicted nitric oxide synthesis was reduced by ZIKV infection through PPAR signaling.

Cytokine signaling can stimulate the breakdown of tight junctions by hindering junction protein synthesis [95]. IPA also predicted many cytokines, including IL-15, IL-27, IL-32, C5, IL-18, and EB13, were significantly up-regulated by ZIKV infection in HSerC. IL-15 was found elevated in the serum of ZIKV-infected patients [96], and important for maintenance of cellular tight junctions [97]. IL-18 and IL-23 levels in serum of ZIKV infected monkeys were also increased [98]. Testicular cells are specialized to control reactive oxygen species levels [99], but higher levels of hydrogen peroxide were predicted to accumulate in ZIKV-infected HSerC, which might be the cause of impaired regulation system. However, the ECIS results (Fig 2) demonstrate that CPE, and hence the predicted breakdown of HSerC tight junctions, takes considerably longer in HSerC than does CPE in permissive Vero cells, the model cells used for ZIKV propagation and titration, which could explain the long-lived persistence of ZIKV in testicular tissues and semen.

Sertoli cells secrete inhibin B, which regulates the expression of FSH, one of the critical regulator hormones for spermatogenesis. Pierik et al. showed that levels of serum inhibin B directly correlate with sperm count, which can be used as a marker for spermatogenesis. Low levels of inhibin B were detected in the serum of infertile males compared to healthy individuals [27]. ZIKV-induced reduction of inhibin B (Fig 5) might be the cause of dysregulated spermatogenesis, resulting in a decrease in sperm count, as observed in previous studies [66].

In conclusion, Sertoli cells support every step of spermatogenesis by providing environmental support, supplying nutrients, and appropriate signals for proliferation and development of germ cells. Any adverse impact on Sertoli cells might affect overall spermatogenesis (modeled in Fig 6), which could result in male infertility. ZIKV infection of Sertoli cells can adversely impact different signaling pathways, bio-functions, cytokines, enzymes, and different cellular proteins that play important roles in spermatogenesis and BTB integrity. For example, activation of the PPAR pathway (Fig 6, upper left) is required for lipid droplet formation and lactate production and metabolism [77, 78, 100]. Thus, PPAR downregulation can negatively affect energy supply. In addition, PGAM1 (Fig 6, left) is a critical enzyme that regulates the glycolysis pathway and plays important roles in cell proliferation, migration and apoptosis [39]. Elevated expression is often associated with cancer [39] and spermatogenic dysfunction [39]. Further studies of these various affected pathways and processes are necessary for a deeper understanding of the impact of ZIKV infection on male and female fertility.

Materials and methods

Cells

Primary human Sertoli cells (HSerC) were purchased from ScienCell Research Laboratories, USA (Catalog #4520). Cells were grown in poly-L-lysine-coated culture vessels in Sertoli Cell Medium (ScienCell Cat. #4521) at 37°C in 5% CO_2. Cells were passaged every 2–3 days by
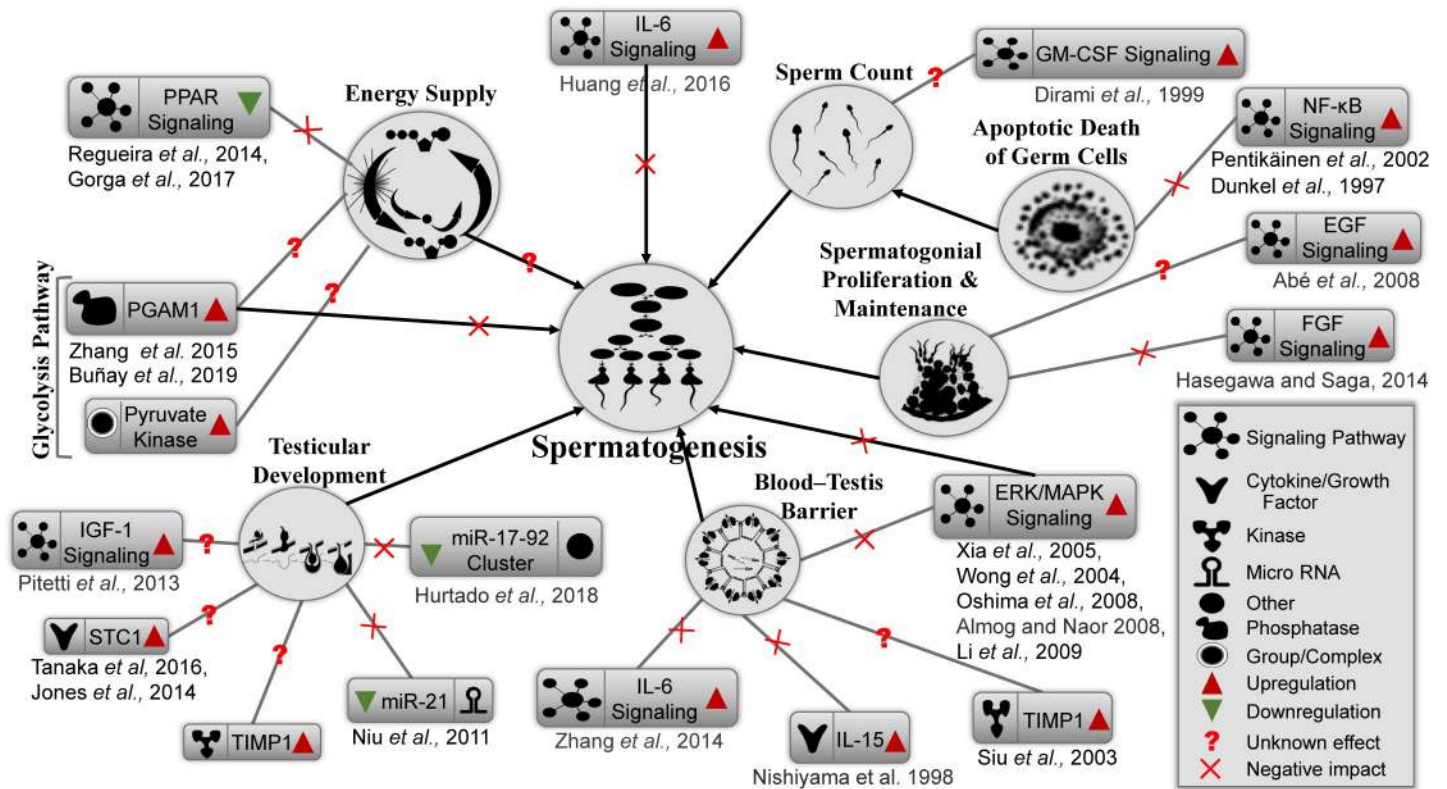
Fig 6. Proposed model for ZIKV-induced impairment of spermatogenesis. ZIKV-induced dysregulation of different proteins and cellular signaling pathways important for spermatogenesis. Energy supply is predicted to be affected by dysregulation of the PPAR signaling and glycolysis pathways. Testicular development could be affected by downregulation of microRNAs and upregulation of STC1, TIMP1, and IGF-1 signaling pathways. BTB integrity could be compromised by upregulation of cytokine (IL-6, IL-15 or ERK/MAPK) signaling pathways. Upregulation of IL-6 and ERK/MAPK signaling could also directly impact the spermatogenesis process. NK-kB and GM-CSF signaling could reduce the sperm count via apoptosis. However, spermatogonial proliferation and maintenance, regulated by EGF and FGF signaling pathway, were significantly upregulated by ZIKV infection, which could also adversely impact the spermatogenesis process.

https://doi.org/10.1371/journal.pntd.0008335.g006

mild trypsinization as recommended by the company. Cells grown to passage 4 were used for all experiments.

Virus

The Zika virus strain from Puerto Rico used in this study (ZIKV/Homo sapiens/PRI/PRVABC59/2015) was a gift from Dr. David Safronetz, Chief of Special Pathogens, the National Microbiology Laboratory, Public Health Agency of Canada. The virus stock was amplified by growing in Vero cells (ATCC #CCL-81) and preserved in 10% FBS at -80˚C for future use. Stock virus titers were determined by plaque assay in Vero cells.

Infection

HSerC were grown to 70% confluency and infected at a multiplicity of infection (MOI) of 0.3 or 3 plaque forming units (PFU) per cell, as detailed in specific experiments. The virus inoculum was adsorbed to cell surface by rocking the culture plates every 15 minutes for 2 hours at 37˚C in a CO_2 incubator, followed by adding fresh Sertoli cell medium. For viral growth curve determinations, supernatants of ZIKV-infected cells were collected every alternating day from day 1 to 9 post-infection. Virus titers in the supernatants were determined by plaque assay. All experiments were done in triplicates.

Cell viability

Cell viability was determined using cell proliferation reagent WST-1 (Roche) according to the manufacturer's protocol. Briefly, HSerC cells were grown in 96 well plates and infected with ZIKV at MOI = 3. Nine μl of WST-1 reagent was added to each well various days post infection and incubated at 37°C for 2 hours. Colorimetric changes were determined by photo-densitometer and cell viability was calculated compared to time-matched non-infected wells. Each experiment was done in 3 biological replicates with 5 technical replicates each time.

Protein extraction and quantification

Assessment of proteomic dysregulation was performed by Western blot and SOMAscan-determined on ZIKV-infected and time-matched mock-treated cells on Day 1, 3 and 5 post-infection (dpi). Cells were scraped from the culture vessels, washed 3 times in ice-cold PBS and lysed by sonication in 60 μl MPER detergent, supplemented with 1× HALT Protease inhibitor solution. Insoluble cellular components were removed by centrifugation at 14,000×g for 10 min at 4°C. The concentrations of proteins in the clear supernatants were determined by BCA Protein Assay (Pierce; Rockford, IL) and quantified using bovine serum albumin standards.

Immunoblotting

Protein concentrations from the cell lysates were measured as described above by BCA assay and 20μg of protein were resolved in SDS-PAGE gels and transferred to 0.2μm nitrocellulose membranes. 12% and 6% gels were used for separation of lower and higher molecular weight proteins, respectively. Rabbit anti-PSMA2 (Cell Signaling, Cat. 2455), anti-THBS2 (Abcam, Cat. ab84469), and anti–CST3 (Abcam, Cat. Ab109508), and mouse anti-ZIKV NS1 (BioFront Technologies Cat. BF-1225-06), anti-caspase 3 (Cell Signaling Cat. 3G2), anti-STAT1 (Cell Signaling, Cat. 9176S) and anti-Beta-Actin (Cell Signaling, Cat. 3700S) primary antibodies were used to detect specific proteins. (HRP)-conjugated horse anti-mouse (Cell Signaling, Cat. #7076) or anti-rabbit (Cell Signaling, Cat. #7074) secondary antibodies were used for detection of the immune complexes. Protein bands were imaged with an Alpha Innotech FluorChemQ MultiImage III after developed with ECL reagents. Band intensities were quantified with Image J 1.50i (USA) and graphically presented by Graphpad Prism software (La Jolla, California, USA).

Photomicrography

ZIKV-infected and mock-treated HSerC cells were examined every alternate day from day 1 to 9 to observe cytopathic effects (CPE) of the virus infection with a Nikon TE-2000 inverted microscope and photographs were taken at 200× magnification with a Canon-A700 digital camera. Slight adjustments were made in brightness and contrast of the images in Power point, which did not alter image context with respect to each other.

Immunofluorescent microscopy

HSerC cells were grown on spotted slides in Sertoli cell media at 37°C for 24 hours, and infected with ZIKV as previously described. Mock-infected cells were used as control. At 1, 3 and 5 dpi, both ZIKV-infected and mock cells were washed 5× with sterile 1× PBS and fixed with 4% paraformaldehyde for 15min. Paraformaldehyde was removed from cells by 5× wash with sterile 1× PBS. Cells were permeabilized with 0.1% TritonX-100 in PBS for 5 mins. 20 μl of 3% bovine serum albumin (BSA) was used overnight at 4°C for blocking. Cells were then incubated with primary anti-ZIKV-NS1 antibody in 3% BSA overnight at 4°C. After overnight

incubation, cells were washed again 5× with sterile PBS and 0.2% Tween 20 (PBT) and incubated for 60min with Alexa Fluor546-tagged anti-mouse secondary antibody for 20min. Finally, cells were mounted with DAPI-containing mounting dye. Slides were imaged using a Zeiss Axio Observer Z1 inverted fluorescence microscope.

SOMAscan analyses

A total of 18 (three biological replicates of each time point) cell lysate samples were collected from mock- and ZIKV-infected HSerC at 1, 3 and 5 dpi. For SOMAscan analysis, the protein concentrations were adjusted to 250 μg/ml. Proteomic analyses was performed on a SomaLogics-licensed platform in the Manitoba Centre for Proteomics and Systems Biology, using a SOMAscan version 1.3 platform capable of measuring 1307 proteins simultaneously from up to 92 samples. During the SOMAscan assay, each biologic sample was mixed with SomaLogic's proprietary SOMAmers. Each of the SOMAmers has the capacity to selectively recognize and bind to a specific human protein [28, 101]. After mixing and binding each sample in an individual 96-well, the SOMAmers are washed, released, hybridized to DNA microarrays and quantified [101, 102]. The expression values are generated as relative fluorescent units (RFU) which are directly proportional to the amounts of target proteins in the initial samples, as confirmed by a standard curve generated for each protein-SOMAmer pair [28, 101].

Electric cell-substrate impedance sensing of ZIKV infections

Cell barrier integrity was tested by electrical impedance as previously described by Nickol *et al.* [103]. Briefly, Vero and HSerC were added to 96-well ECIS plates (Applied Biosystems) and rested at 32°C/ 5% CO_2 for 24 hours until confluent monolayers were formed. Cells were then treated with media alone (mock-infected positive control), 1% Triton X-100 (negative control), or with ZIKV at MOI of 0.3 or 3.0. Electrical impedance of the cultures was continually monitored from 24 hours before treatment to 90 hours post-treatment. Values for each treatment were determined from a minimum of 8 wells, and the HSerC were tested twice.

Inhibin B levels detection

HSerC were infected with ZIKV (MOI 3) and induced with 62.5ng/ml or 125ng/ml follicular stimulating hormone (FSH) (Sigma-Aldrich, Canada, Cat. F4021). Mock-infected and FSH-treated or untreated HSerC were used as control. Cell culture supernatants were collected after 48 hours post-infection and stored at -20°C before analyzing. The inhibin B level was determined using manufacturers' recommendations, inhibin-B ELISA kit (Sigma-Aldrich, Canada, Cat. RAB0325). This assay has an inter-plate CV <15%, and intra-plate CV <10%, with minimum detection limit of 2pg/ml (n = 3 assays). The fold difference of inhibin B expression was determined by dividing by Mock-infected inhibin B concentration.

Statistical and bioinformatics analyses

Data from the 18 ZIKV-infected and time-matched mock samples were imported into Excel and converted to Log_2 values. Fold-changes of each of the proteins in each infected sample were determined by comparing each to its time-matched mock sample. Students T-test (2 tails) and Z-score analyses were done to quantify the p-value from the fold-changes, as described [104]. Average 1.3-fold and 1.5-fold dysregulation with p-value <0.05 were examined and cutoff of 1.3-fold was set for further analyses (S1 Table) by Ingenuity Pathway Analysis (IPA) and PANTHER. Any protein with a fold-change value beyond the 1.3-fold cutoff, but considered non-significant by T-test, was re-examined by Z-score analysis. The Z-scores from

each replicate were determined, and cutoffs of $\geq 1.96\sigma$ or $\leq -1.96\sigma$ were considered significant. At least two of the replicates had to have significant Z-score values of the same trend (*e.g.* if up-regulated, two or more values must be $>1.96\sigma$, the 3rd replicate must have a Z-score $> 0.98\sigma$, and the overall average must be $\geq 1.96\sigma$). P-values for these were calculated from the average of the three Z-scores.

Supporting information

S1 Fig. Heat map of differentially expressed (fold change > 1.33 or < -1.33) proteins at 1, 3 and 5 days post ZIKV infection. Up- and down-regulated proteins are highlighted in red and blue, respectively.
(PDF)

S2 Fig. Expression of significantly dysregulated proteins in molecular pathways at 1, 3 and 5 dpi. The datasets containing protein IDs, fold changes, and P-values were imported into IPA, and interacting pathways assembled for differentially expressed proteins. Up- and down-regulated proteins are indicated in red and green, respectively; gray were identified in this study but not affected; colorless proteins interact with various proteins in the pathway but are not recognized by the SOMA panel.
(PDF)

S3 Fig. IPA-generated molecular networks of dysregulated proteins at 3 and 5 dpi. The datasets containing protein IDs, fold changes, and P-values were imported into the IPA software, and interacting networks were assembled for differentially expressed proteins at 3 and 5 dpi. Up- and down-regulated proteins are indicated in red and green, respectively; gray proteins denote those that were identified in this study but not dysregulated; colorless proteins interact with various proteins in the pathway but were not recognized in our screening.
(PDF)

S4 Fig. Gene ontology (GO) analysis of up- and down-regulated proteins. Up- and down-regulated proteins were analysed by PANTHER and GOTERM database separately, and their associations to biological processes, molecular functions, and cellular components determined. Up-regulated and down-regulated protein functions at 3 and 5 dpi are listed in a, b, c, and d respectively.
(PDF)

S5 Fig. Cellular impact of the most highly dysregulated proteins (± Fold change > 5.0, p ≤ 0.05) in ZIKV-infected HSerC. The most affected cellular network predicted by IPA at 3 dpi, shown at (**A**) 3 dpi and at (**B**) 5 dpi. (**C**) Disease and functions predicted significantly dysregulated at 5 dpi by most dysregulated proteins. (**D**) List of most dysregulated proteins at 3 and 5 dpi.
(PDF)

S1 Table. List of proteins dysregulated at least 1.3-fold and significant by T-Test (p-value < 0.05) or Z-score ($\geq 1.96\sigma$ or $\leq -1.96\sigma$). dpi = days post infection, red = significantly up-regulated; green = significantly down-regulated; purple = p value < 0.05. Table sorted first by significantly up-regulated proteins at day 1 post-infection, then by those significantly down-regulated at 1dpi; then by significantly up- and down-regulated at 3dpi; then by significantly up- and down-regulated at 5dpi.
(XLSX)

S2 Table. List of the most highly dysregulated IPA-determined "Diseases & Functions" at 3dpi and at 5dpi, with individual proteins assigned to each function depicted in red if significantly up-regulated, or in green if significantly down-regulated. Table sorted by each day, then according to default IPA score setting.
(XLSX)

S3 Table. List of IPA-predicted significantly activated or inhibited Sertoli cell "Diseases and Functions" affected by ZIKV infection. Only those with predicted significantly affected activation or inhibition are indicated, in red or green, respectively. Table sorted first by whether Disease or Function activation state is decreased (in green) or increased (in red), then by p-value.
(XLSX)

S4 Table. List of IPA-determined "Disease or Cellular Functions" significantly dysregulated by ZIKV infection at 5 dpi. Only those with predicted significantly affected activation or inhibition are indicated, in red or green, respectively. Table sorted first by Category name, then by p-value, then by whether Disease or Function activation state is increased (in red) or decreased (in green).
(XLSX)

Author Contributions

Conceptualization: Jason Kindrachuk, John A. Wilkins, Kevin M. Coombs.

Formal analysis: Mahamud-ur Rashid, Ali Zahedi-Amiri, Kathleen K. M. Glover, Ang Gao, Jason Kindrachuk, John A. Wilkins, Kevin M. Coombs.

Funding acquisition: Jason Kindrachuk, John A. Wilkins, Kevin M. Coombs.

Investigation: Mahamud-ur Rashid, Ali Zahedi-Amiri, Kathleen K. M. Glover, Ang Gao, Michaela E. Nickol.

Project administration: Kevin M. Coombs.

Supervision: Jason Kindrachuk, John A. Wilkins, Kevin M. Coombs.

Validation: Kathleen K. M. Glover.

Visualization: Mahamud-ur Rashid, Ali Zahedi-Amiri, Kathleen K. M. Glover, Michaela E. Nickol.

Writing – original draft: Mahamud-ur Rashid.

Writing – review & editing: Mahamud-ur Rashid, Ali Zahedi-Amiri, Kathleen K. M. Glover, Ang Gao, Michaela E. Nickol, Jason Kindrachuk, John A. Wilkins, Kevin M. Coombs.

References

1. Laureti M, Narayanan D, Rodriguez-Andres J, Fazakerley JK, Kedzierski L. Flavivirus receptors: Diversity, identity, and cell entry. Front Immunol. 2018; 9. Artn 2180 https://doi.org/10.3389/fimmu.2018.02180 ISI:000445660900001. PMID: 30319635

2. Vasilakis N, Weaver SC. Flavivirus transmission focusing on Zika. Curr Opin Virol. 2017; 22:30–5. https://doi.org/10.1016/j.coviro.2016.11.007 ISI:000397374300007. PMID: 27936448

3. Wikan N, Smith DR. Zika virus: history of a newly emerging arbovirus. Lancet Infect Dis. 2016; 16(7): E119–E26. https://doi.org/10.1016/S1473-3099(16)30010-X ISI:000378319600002. PMID: 27282424

4. Lessler J, Chaisson LH, Kucirka LM, Bi QF, Grantz K, Salje H, et al. Assessing the global threat from Zika virus. Science. 2016; 353(6300). ARTN aaf8160 https://doi.org/10.1126/science.aaf8160 ISI:000381561200031. PMID: 27417495

5. Ribeiro LS, Marques RE, de Jesus AMR, de Almeida RP, Teixeira MM. Zika crisis in Brazil: challenges in research and development. Curr Opin Virol. 2016; 18:76–81. https://doi.org/10.1016/j.coviro.2016.04.002 ISI:000382273200014. PMID: 27179929

6. Baud D, Gubler DJ, Schaub B, Lanteri MC, Musso D. An update on Zika virus infection. Lancet. 2017; 390(10107):2099–109. https://doi.org/10.1016/S0140-6736(17)31450-2 ISI:000414250800027. PMID: 28647173

7. Zika situation report [Internet]. 2017 [cited 25 August 2017]. Available from: http://www.who.int/emergencies/zika-virus/situation-report/25-august-2016/en/.

8. Petersen LR, Jamieson DJ, Powers AM, Honein MA. Zika virus. New Engl J Med. 2016; 374 (16):1552–63. https://doi.org/10.1056/NEJMra1602113 ISI:000374383900008. PMID: 27028561

9. Faye O, Freire CCDM, Faye O, de Oliveira JV, Zanotto PMDA, Diallo M, et al. Molecular evolution of Zika virus during its emergence in the 20th century. Int J Infect Dis. 2014; 21:2–3. https://doi.org/10.1016/j.ijid.2014.03.411 ISI:000209704000005.

10. Brooks RB, Carlos MP, Myers RA, White MG, Bobo-Lenoci T, Aplan D, et al. Likely sexual transmission of Zika virus from a man with no symptoms of infection—Maryland, 2016. Mmwr-Morbid Mortal W. 2016; 65(34):915–6. https://doi.org/10.15585/Mmwr.Mm6534e2 ISI:000382902700007. PMID: 27585037

11. Deckard DT, Chung WM, Brooks JT, Smith JC, Woldai S, Hennessey M, et al. Male-to-male sexual transmission of Zika virus—Texas, January 2016. Mmwr-Morbid Mortal W. 2016; 65(14):372–4. https://doi.org/10.15585/Mmwr.Mm6514a3 ISI:000374633200003.

12. Tang WW, Young MP, Mamidi A, Regla-Nava JA, Kim K, Shresta S. A mouse model of Zika virus sexual transmission and vaginal viral replication. Cell Reports. 2016; 17(12):3091–8. https://doi.org/10.1016/j.celrep.2016.11.070 ISI:000390895600001. PMID: 28009279

13. Counotte MJ, Kim CR, Wang JY, Bernstein K, Deal CD, Broutet NJN, et al. Sexual transmission of Zika virus and other flaviviruses: A living systematic review. PLoS Med. 2018; 15(7). ARTN e1002611 https://doi.org/10.1371/journal.pmed.1002611 ISI:000440339700018. PMID: 30040845

14. Medina FA, Torres G, Acevedo J, Fonseca S, Casiano L, De Leon C, et al. Duration of infectious Zika virus. Am J Trop Med Hyg. 2018; 99(4):298–. ISI:000461386603283.

15. Nicastri E, Castilletti C, Liuzzi G, Iannetta M, Capobianchi MR, Ippolito G. Persistent detection of Zika virus RNA in semen for six months after symptom onset in a traveller returning from Haiti to Italy, February 2016. Eurosurveillance. 2016; 21(32):6–9. Artn 30314 https://doi.org/10.2807/1560-7917.Es.2016.21.32.30314 ISI:000382228800002. PMID: 27541989

16. Sheng ZY, Gao N, Wang ZY, Cui XY, D.S. Z, D.Y. F, et al. Sertoli cells are susceptible to ZIKV infection in mouse testis. Front Cell Infect Microbiol. 2017; 7:272. https://doi.org/10.3389/fcimb.2017.00272 PMID: 28680856

17. Govero J, Esakky P, Scheaffer SM, Fernandez E, Drury A, Platt DJ, et al. Zika virus infection damages the testes in mice. Nature. 2016; 540(7633):438–+. https://doi.org/10.1038/nature20556 ISI:000389716800043. PMID: 27798603

18. Kumar A, Jovel J, Lopez-Orozco J, Limonta D, Airo AM, Hou SM, et al. Human Sertoli cells support high levels of Zika virus replication and persistence. Sci Rep. 2018; 8:5477. Artn 5477 https://doi.org/10.1038/s41598-018-23899-x ISI:000428999200013. PMID: 29615760

19. Matusali G, Houzet L, Satie AP, Mahe D, Aubry F, Couderc T, et al. Zika virus infects human testicular tissue and germ cells. J Clin Invest. 2018; 128(10):4697–710. https://doi.org/10.1172/JCI121735 ISI:000446063600046. PMID: 30063220

20. Griswold MD. 50 years of spermatogenesis: Sertoli cells and their interactions with germ cells. Biol Reprod. 2018; 99(1):87–100. https://doi.org/10.1093/biolre/ioy027 ISI:000446329200008. PMID: 29462262

21. Oatley JM, Brinster RL. The germline stem cell niche unit in mammalian testes. Physiol Rev. 2012; 92 (2):577–95. https://doi.org/10.1152/physrev.00025.2011 ISI:000306562500003. PMID: 22535892

22. Riera MF, Galardo MN, Pellizzari EH, Meroni SB, Cigorraga SB. Molecular mechanisms involved in Sertoli cell adaptation to glucose deprivation. Am J Physiol-Endoc M. 2009; 297(4):E907–E14. https://doi.org/10.1152/ajpendo.00235.2009 ISI:000270139400009. PMID: 19638510

23. Jutte NHPM, Eikvar L, Levy FO, Hansson V. Metabolism of palmitate in cultured rat Sertoli cells. J Reprod Fertil. 1985; 73(2):497–503. ISI:A1985AFU1900026. https://doi.org/10.1530/jrf.0.0730497 PMID: 4039365

24. Lucas TF, Nascimento AR, Pisolato R, Pimenta MT, Lazari MFM, Porto CS. Receptors and signaling pathways involved in proliferation and differentiation of Sertoli cells. Spermatogenesis. 2014; 4(1): e28138.

25. Oduwole OO, Peltoketo H, Huhtaniemi IT. Role of Follicle-Stimulating Hormone in Spermatogenesis. Front Endocrinol. 2018; 9. ARTN 763 https://doi.org/10.3389/fendo.2018.00763 WOS:000453395300001. PMID: 30619093

26. Okuma Y, O'Connor AE, Muir JA, Stanton PG, de Kretser DM, Hedger MP. Regulation of activin A and inhibin B secretion by inflammatory mediators in adult rat Sertoli cell cultures. J Endocrinol. 2005; 187 (1):125–34. https://doi.org/10.1677/joe.1.06266 WOS:000232714200013. PMID: 16214948

27. Pierik FH, Vreeburg JTM, Stijnen T, de Jong FH, Weber RFA. Serum inhibin B as a marker of sper-matogenesis. J Clin Endocr Metab. 1998; 83(9):3110–4. https://doi.org/10.1210/jcem.83.9.5121 WOS:000075840700018. PMID: 9745412

28. Candia J, Cheung F, Kotliarov Y, Fantoni G, Sellers B, Griesman T, et al. Assessment of variability in the SOMAscan assay. Sci Rep. 2017; 7. Artn 14248 https://doi.org/10.1038/S41598-017-14755-5 ISI:000413907000071. PMID: 29079756

29. Foy BD, Kobylinski KC, Foy JLC, Blitvich BJ, da Rosa AT, Haddow AD, et al. Probable non-vector-borne transmission of Zika virus, Colorado, USA. Emerg Infect Dis. 2011; 17(5):880–2. https://doi.org/10.3201/eid1705.101939 ISI:000290291900020. PMID: 21529401

30. Moreira J, Peixoto TM, Siqueira AM, Lamas CC. Sexually acquired Zika virus: a systematic review. Clin Microbiol Infect. 2017; 23(5):296–305. https://doi.org/10.1016/j.cmi.2016.12.027 ISI:000404469900007. PMID: 28062314

31. Atkinson B, Thorburn F, Petridou C, Bailey D, Hewson R, Simpson AJH, et al. Presence and persis-tence of Zika virus RNA in semen, United Kingdom, 2016. Emerg Infect Dis. 2017; 23(4):611–5. https://doi.org/10.3201/eid2304.161692 ISI:000396824400007. PMID: 27997333

32. Duggal NK, Ritter JM, Pestorius SE, Zaki SR, Davis BS, Chang GJJ, et al. Frequent Zika virus sexual transmission and prolonged viral RNA shedding in an immunodeficient mouse model. Cell Reports. 2017; 18(7):1751–60. https://doi.org/10.1016/j.celrep.2017.01.056 ISI:000397324900016. PMID: 28199846

33. Ma WQ, Li SH, Ma SQ, Jia LN, Zhang FC, Zhang Y, et al. Zika virus causes testis damage and leads to male infertility in mice. Cell. 2016; 167(6):1511–+. https://doi.org/10.1016/j.cell.2016.11.016 ISI:000389470500014. PMID: 27884405

34. Siddharthan V, Van Wettere AJ, Li R, Miao JX, Wang ZD, Morrey JD, et al. Zika virus infection of adult and fetal STAT2 knock-out hamsters. Virology. 2017; 507:89–95. https://doi.org/10.1016/j.virol.2017.04.013 ISI:000402218500010. PMID: 28431283

35. Osuna CE, Lim SY, Deleage C, Griffin BD, Stein D, Schroeder LT, et al. Zika viral dynamics and shed-ding in rhesus and cynomolgus macaques. Nat Med. 2016; 22(12):1448–+. https://doi.org/10.1038/nm.4206 ISI:000389549000022. PMID: 27694931

36. Hirsch AJ, Smith JL, Haese NN, Broeckel RM, Parkins CJ, Kreklywich C, et al. Zika virus infection of rhesus macaques leads to viral persistence in multiple tissues. PLoS Path. 2017; 13(3). ARTN e1006219 https://doi.org/10.1371/journal.ppat.1006219 ISI:000398120300031. PMID: 28278237

37. Siemann DN, Strange DP, Maharaj PN, Shi PY, Verma S. Zika virus infects human Sertoli cells and modulates the integrity of the in vitro blood-testis barrier model. J Virol. 2017; 91(22):e00623–17. UNSP e00623-17 https://doi.org/10.1128/JVI.00623-17 ISI:000414005400003. PMID: 28878076

38. Robinson CL, Chong ACN, Ashbrook AW, Jeng G, Jin JL, Chen HQ, et al. Male germ cells support long-term propagation of Zika virus. Nat Commun. 2018; 9. Artn 2090 https://doi.org/10.1038/S41467-018-04444-W ISI:000433297900001. PMID: 29844387

39. Zhang SB, Zhao YS, Lei B, Li CJ, Mao XM. PGAM1 is involved in spermatogenic dysfunction and affects cell proliferation, apoptosis, and migration. Reprod Sci. 2015; 22(10):1236–42. https://doi.org/10.1177/1933719115572485 ISI:000361530300007. PMID: 25701843

40. Hitosugi T, Zhou L, Elf S, Fan J, Kang HB, Seo JH, et al. Phosphoglycerate mutase 1 coordinates gly-colysis and biosynthesis to promote tumor growth. Cancer Cell. 2012; 22(5):585–600. https://doi.org/10.1016/j.ccr.2012.09.020 ISI:000311181200006. PMID: 23153533

41. Jiang XL, Sun Q, Li H, Li K, Ren XB. The role of phosphoglycerate mutase 1 in tumor aerobic glycoly-sis and its potential therapeutic implications. Int J Cancer. 2014; 135(9):1991–6. https://doi.org/10.1002/ijc.28637 ISI:000341983700004. PMID: 24285383

42. Wen YA, Zhou BW, Lv DJ, Shu FP, Song XL, Huang B, et al. Phosphoglycerate mutase 1 knockdown inhibits prostate cancer cell growth, migration, and invasion. Asian J Androl. 2018; 20(2):178–83. https://doi.org/10.4103/aja.aja_57_17 ISI:000426995900014. PMID: 29271400

43. Bunay J, Larriba E, Patino-Garcia D, Urriola-Munoz P, Moreno RD, del Mazo J. Combined proteomic and miRNome analyses of mouse testis exposed to an endocrine disruptors chemicals mixture reveals altered toxicological pathways involved in male infertility. Mol Human Reprod. 2019; 25(3):156–69. https://doi.org/10.1093/molehr/gaz003 ISI:000461154600005. PMID: 30698749

44. Brew K, Dinakarpandian D, Nagase H. Tissue inhibitors of metalloproteinases: evolution, structure and function. BBA-Protein Struct M. 2000; 1477(1–2):267–83. https://doi.org/10.1016/S0167-4838(99)00279-4 ISI:000085998500021.

45. Baumgart E, Lenk SV, Loening SA, Jung K. Tissue inhibitors of metalloproteinases 1 and 2 in human seminal plasma and their association with spermatozoa. Int J Androl. 2002; 25(6):369–71. https://doi.org/10.1046/j.1365-2605.2002.00383.x ISI:000178841600007. PMID: 12406369

46. Shimokawa K, Katayama M, Matsuda Y, Takahashi H, Hara I, Sato H, et al. Matrix metalloproteinase (MMP)-2 and MMP-9 activities in human seminal plasma. Mol Human Reprod. 2002; 8(1):32–6. https://doi.org/10.1093/molehr/8.1.32 ISI:000173544100005.

47. Belardin LB, Antoniassi MP, Camargo M, Intasqui P, Fraietta R, Bertolla RP. Semen levels of matrix metalloproteinase (MMP) and tissue inhibitor of metalloproteinases (TIMP) protein families members in men with high and low sperm DNA fragmentation. Sci Rep. 2019; 9. Artn 10234 https://doi.org/10.1038/S41598-019-45361-2 ISI:000474732300001. PMID: 31292458

48. Siu MKY, Lee WM, Cheng CY. The interplay of collagen IV, tumor necrosis factor-alpha, gelatinase B (matrix metalloprotease-9), and tissue inhibitor of metalloproteases-1 in the basal lamina regulates Sertoli cell-tight junction dynamics in the rat testis. Endocrinology. 2003; 144(1):371–87. https://doi.org/10.1210/en.2002-220786 ISI:000180176100046. PMID: 12488366

49. Siu MK, Cheng CY. Extracellular matrix and its role in spermatogenesis. In: Cheng CY, editor. Molecular mechanisms in spermatogenesis, Advances in Experimental Medicine and Biology. 636: Springer, New York; 2009. p. 74–91.

50. Anfasa F, Siegers JY, van der Kroeg M, Mumtaz N, Raj VS, de Vrij FMS, et al. Phenotypic differences between Asian and African lineage Zika viruses in human neural progenitor cells. mSphere. 2017; 2(4):e00292–17. ARTN e00292-17 https://doi.org/10.1128/mSphere.00292-17 ISI:000408618500028. PMID: 28815211

51. Vincent ZL, Mitchell MD, Ponnampalam AP. Regulation of TIMP-1 in human placenta and fetal membranes by lipopolysaccharide and demethylating agent 5-aza-2 '-deoxycytidine. Reprod Biol Endocrin. 2015;13. Artn 136 https://doi.org/10.1186/S12958-015-0132-Y ISI:000367048900001. PMID: 26691525

52. VadilloOrtega F, Hernandez A, GonzalezAvila G, Bermejo L, Iwata K, Strauss JF. Increased matrix metalloproteinase activity and reduced tissue inhibitor of metalloproteinases-1 levels in amniotic fluids from pregnancies complicated by premature rupture of membranes. Am J Obstet Gynecol. 1996; 174(4):1371–6. https://doi.org/10.1016/s0002-9378(96)70687-7 ISI:A1996UH18400055. PMID: 8623872

53. Lind AK, Dahm-Kahler P, Weijdegard B, Sundfeldt K, Brannstrom M. Gelatinases and their tissue inhibitors during human ovulation: increased expression of tissue inhibitor of matrix metalloproteinase-1. Mol Human Reprod. 2006; 12(12):725–36. https://doi.org/10.1093/molehr/gal086 ISI:000242272100002. PMID: 17071711

54. Li MWM, Mruk DD, Cheng CY. Mitogen-activated protein kinases in male reproductive function. Trends Mol Med. 2009; 15(4):159–68. https://doi.org/10.1016/j.molmed.2009.02.002 ISI:000265988200003. PMID: 19303360

55. Malm J, He XH, Bjartell A, Shen L, Abrahamsson PA, Dahlback B. Vitamin-K-dependent protein-S in Leydig-cells of human testis. Biochem J. 1994; 302:845–50. https://doi.org/10.1042/bj3020845 ISI:A1994PJ33700030. PMID: 7945211

56. Lumbroso D, Soboh S, Maimon A, Schif-Zuck S, Ariel A, Burstyn-Cohen T. Macrophage-derived protein S facilitates apoptotic polymorphonuclear cell clearance by resolution phase macrophages and supports their reprogramming. Front Immunol. 2018; 9. Artn 358 https://doi.org/10.3389/Fimmu.2018.00358 ISI:000426380600001. PMID: 29545796

57. Zhou W, Bolden-Tiller OU, Shao SH, Weng CC, Shetty G, AbuElhija M, et al. Estrogen-regulated genes in rat testes and their relationship to recovery of spermatogenesis after irradiation. Biol Reprod. 2011; 85(4):823–33. https://doi.org/10.1095/biolreprod.111.091611 ISI:000295457200020. PMID: 21653891

58. Jones S, Boisvert A, Duong TB, Francois S, Thrane P, Culty M. Disruption of rat testis development following combined in utero exposure to the phytoestrogen Genistein and antiandrogenic plasticizer di-(2-ethylhexyl) phthalate. Biol Reprod. 2014; 91(3). ARTN 64 https://doi.org/10.1095/biolreprod.114.120907 ISI:000341600400010. PMID: 25031359

59. Tanaka T, Kanatsu-Shinohara M, Lei ZM, Rao CV, Shinohara T. The luteinizing hormone-testosterone pathway regulates mouse spermatogonial stem cell self-renewal by suppressing WNT5A expression in Sertoli cells. Stem Cell Rep. 2016; 7(2):279–91. https://doi.org/10.1016/j.stemcr.2016.07.005 ISI:000381380900012. PMID: 27509137

60. Uuskula L, Mannik J, Rull K, Minajeva A, Koks S, Vaas P, et al. Mid-gestational gene expression profile in placenta and link to pregnancy complications. PLoS One. 2012; 7(11). ARTN e49248 https://doi.org/10.1371/journal.pone.0049248 ISI:000311935800237. PMID: 23145134

61. Batiz LF, De Blas GA, Michaut MA, Ramirez AR, Rodriguez F, Ratto MH, et al. Sperm from Hyh mice carrying a point mutation in alpha SNAP have a defect in acrosome reaction. PLoS One. 2009; 4(3). ARTN e4963 https://doi.org/10.1371/journal.pone.0004963 ISI:000265498800011. PMID: 19305511

62. Arcos A, de Paola M, Gianetti D, Acuna D, Velasquez ZD, Miro MP, et al. alpha-SNAP is expressed in mouse ovarian granulosa cells and plays a key role in folliculogenesis and female fertility. Sci Rep. 2017; 7. Artn 11765 https://doi.org/10.1038/S41598-017-12292-9 ISI:000410916100023. PMID: 28924180

63. Huang GZ, Yuan M, Zhang J, Li J, Gong D, Li YY, et al. IL-6 mediates differentiation disorder during spermatogenesis in obesity-associated inflammation by affecting the expression of Zfp637 through the SOCS3/STAT3 pathway. Sci Rep. 2016; 6. Artn 28012 https://doi.org/10.1038/Srep28012 ISI:000378219000001. PMID: 27329259

64. Zhang HJ, Yin YM, Wang GS, Liu ZM, Liu L, Sun F. Interleukin-6 disrupts blood-testis barrier through inhibiting protein degradation or activating phosphorylated ERK in Sertoli cells. Sci Rep. 2014; 4. Artn 4260 https://doi.org/10.1038/Srep04260 ISI:000332067200001.

65. Pitetti JL, Calvel P, Zimmermann C, Conne B, Papaioannou MD, Aubry F, et al. An essential role for insulin and IGF1 receptors in regulating Sertoli cell proliferation, testis size, and FSH action in mice. Mol Endocrinol. 2013; 27(5):814–27. https://doi.org/10.1210/me.2012-1258 ISI:000318154400010. PMID: 23518924

66. Joguet G, Mansuy JM, Matusali G, Hamdi S, Walschaerts M, Pavili L, et al. Effect of acute Zika virus infection on sperm and virus clearance in body fluids: a prospective observational study. Lancet Infect Dis. 2017; 17(11):1200–8. https://doi.org/10.1016/S1473-3099(17)30444-9 ISI:000414059800043. PMID: 28838639

67. Dirami G, Ravindranath N, Pursel V, Dym M. Effects of stem cell factor and granulocyte macrophage-colony stimulating factor on survival of porcine type A spermatogonia cultured in KSOM. Biol Reprod. 1999; 61(1):225–30. https://doi.org/10.1095/biolreprod61.1.225 ISI:000081150200030. PMID: 10377053

68. Abe K, Eto K, Abe S. Epidermal growth factor mediates spermatogonial proliferation in newt testis. Reprod Biol Endocrin. 2008; 6. Artn 7 https://doi.org/10.1186/1477-7827-6-7 ISI:000254442100001. PMID: 18254942

69. Dunkel L, Hirvonen V, Erkkila K. Clinical aspects of male germ cell apoptosis during testis development and spermatogenesis. Cell Death Differ. 1997; 4(3):171–9. https://doi.org/10.1038/sj.cdd.4400234 ISI:A1997WR52800002. PMID: 16465226

70. Delfino F, Walker WH. Stage-specific nuclear expression of NF-kappa B in mammalian testis. Mol Endocrinol. 1998; 12(11):1696–707. https://doi.org/10.1210/mend.12.11.0194 ISI:000076679300005. PMID: 9817596

71. Pentikainen V, Suomalainen L, Erkkila K, Martelin E, Parvinen M, Pentikainen MO, et al. Nuclear factor-kappa B activation in human testicular apoptosis. Am J Pathol. 2002; 160(1):205–18. https://doi.org/10.1016/s0002-9440(10)64364-7 ISI:000173231700024. PMID: 11786414

72. Cotton LM, O'Bryan MK, Hinton BT. Cellular signaling by fibroblast growth factors (FGFs) and their receptors (FGFRs) in male reproduction. Endocr Rev. 2008; 29(2):193–216. https://doi.org/10.1210/er.2007-0028 ISI:000254641000003. PMID: 18216218

73. Hasegawa K, Saga Y. FGF8-FGFR1 signaling acts as a niche factor for maintaining undifferentiated spermatogonia in the mouse. Biol Reprod. 2014; 91(6). ARTN 145 https://doi.org/10.1095/biolreprod.114.121012 ISI:000355603600003. PMID: 25359900

74. Suzuki K, Tokue A, Kamiakito T, Kuriki K, Saito K, Tanaka A. Predominant expression of fibroblast growth factor (FGF) 8, FGF4, and FGF receptor 1 in nonseminomatous and highly proliferative components of testicular germ cell tumours. Virchows Arch. 2001; 439(5):616–21. https://doi.org/10.1007/s004280100437 ISI:000172511300004. PMID: 11764380

75. Jaillard C, Chatelain PG, Saez JM. Invitro regulation of pig Sertoli-cell growth and function—Effects of fibroblast growth-factor and somatomedin-C. Biol Reprod. 1987; 37(3):665–74. https://doi.org/10.1095/biolreprod37.3.665 ISI:A1987K676700022. PMID: 3118982

76. Almog T, Naor Z. Mitogen activated protein kinases (MAPKs) as regulators of spermatogenesis and spermatozoa functions. Mol Cell Endocrinol. 2008; 282(1–2):39–44. https://doi.org/10.1016/j.mce.2007.11.011 ISI:000254776900007. PMID: 18177996

77. Alves MG, Oliveira PF. Sertoli cells methods and protocols. In: Alves MG, Oliveira PF, editors. Sertoli Cells. 1748: Humana Press; 2018. p. 297 pages.

78. Gorga A, Rindone GM, Regueira M, Pellizzari EH, Camberos MC, Cigorraga SB, et al. PPAR gamma activation regulates lipid droplet formation and lactate production in rat Sertoli cells. Cell Tissue Res. 2017; 369(3):611–24. https://doi.org/10.1007/s00441-017-2615-y ISI:000408949700014. PMID: 28432465

79. Blanco A, Zinkham WH. Lactate dehydrogenases in human testes. Science. 1963; 139(355):601–&. https://doi.org/10.1126/science.139.3555.601 ISI:A19633045C00040. PMID: 17788300

80. Santiemma V, Salfi V, Casasanta N, Fabbrini A. Lactate-dehydrogenase and malate-dehydrogenase of Sertoli cells in rats. Arch Andrology. 1987; 19(1):59–64. https://doi.org/10.3109/01485018708986800 ISI:A1987K693300007. PMID: 3122678

81. Hayashi K, Lopes SMCD, Kaneda M, Tang FC, Hajkova P, Lao KQ, et al. MicroRNA biogenesis is required for mouse primordial germ cell development and spermatogenesis. PLoS One. 2008; 3(3). ARTN e1738 https://doi.org/10.1371/journal.pone.0001738 ISI:000260586600033. PMID: 18320056

82. Papaioannou MD, Nef S. microRNAs in the testis: Building up male fertility. J Androl. 2010; 31(1):26–33. https://doi.org/10.2164/jandrol.109.008128 ISI:000274938700005. PMID: 19875496

83. Procopio MS, de Avelar GF, Costa GMJ, Lacerda SMSN, Resende RR, de Franca LR. MicroRNAs in Sertoli cells: implications for spermatogenesis and fertility. Cell Tissue Res. 2017; 370(3):335–46. https://doi.org/10.1007/s00441-017-2667-z ISI:000416358400001. PMID: 28779347

84. Niu ZY, Goodyear SM, Rao S, Wu X, Tobias JW, Avarbock MR, et al. MicroRNA-21 regulates the self-renewal of mouse spermatogonial stem cells. P Natl Acad Sci USA. 2011; 108(31):12740–5. https://doi.org/10.1073/pnas.1109987108 ISI:000293385700044. PMID: 21768389

85. Hurtado A, Real FM, Palomino R, Carmona FD, Burgos M, Jimenez R, et al. Sertoli cell-specific abla-tion of miR-17-92 cluster significantly alters whole testis transcriptome without apparent phenotypic effects. PLoS One. 2018; 13(5). ARTN e0197685 https://doi.org/10.1371/journal.pone.0197685 ISI:000433084300060. PMID: 29795630

86. Wong CH, Mruk DD, Lui WY, Cheng CY. Regulation of blood-testis barrier dynamics: an in vivo study. J Cell Sci. 2004; 117(5):783–98. https://doi.org/10.1242/jcs.00900 ISI:000189248400014. PMID: 14734653

87. Xia WL, Cheng CY. TGF-beta 3 regulates anchoring junction dynamics in the seminiferous epithelium of the rat testis via the Ras/ERK signaling pathway: An in vivo study. Dev Biol. 2005; 280(2):321–43. https://doi.org/10.1016/j.ydbio.2004.12.036 ISI:000228377600006. PMID: 15882576

88. Oshima T, Miwa H, Joh T. Aspirin induces gastric epithelial barrier dysfunction by activating p38 MAPK via claudin-7. Am J Physiol-Cell Ph. 2008; 295(3):C800–C6. https://doi.org/10.1152/ajpcell.00157.2008 ISI:000258995000024. PMID: 18667601

89. Albarnaz JD, De Oliveira LC, Torres AA, Palhares RM, Casteluber MC, Rodrigues CM, et al. MEK/ERK activation plays a decisive role in yellow fever virus replication: Implication as an antiviral thera-peutic target. Antiviral Res. 2014; 111:82–92. https://doi.org/10.1016/j.antiviral.2014.09.004 ISI:000345185100013. PMID: 25241249

90. Scaturro P, Stukalov A, Haas DA, Cortese M, Draganov K, Plaszczyca A, et al. An orthogonal proteo-mic survey uncovers novel Zika virus host factors. Nature. 2018; 561:253–7. https://doi.org/10.1038/s41586-018-0484-5 PMID: 30177828

91. Strange DP, Green R, Siemann DN, Gale M, Verma S. Immunoprofiles of human Sertoli cells infected with Zika virus reveals unique insights into host-pathogen crosstalk. Sci Rep. 2018; 8. Artn 8702 https://doi.org/10.1038/S41598-018-27027-7 ISI:000434376700004. PMID: 29880853

92. Zhao LJ, Wang W, Ren H, Qi ZT. ERK signaling is triggered by hepatitis C virus E2 protein through DC-SIGN. Cell Stress Chaperones. 2013; 18(4):495–501. https://doi.org/10.1007/s12192-013-0405-3 ISI:000320339700010. PMID: 23378214

93. Sreekanth GP, Yenchitsomanus PT, Limjindaporn T. Role of mitogen-activated protein kinase signal-ing in the pathogenesis of dengue virus infection. Cell Signal. 2018; 48:64–8. https://doi.org/10.1016/j.cellsig.2018.05.002 ISI:000435622700007. PMID: 29753850

94. Lee NPY, Cheng CY. Regulation of Sertoli cell tight junction dynamics in the rat testis via the nitric oxide synthase/soluble guanylate cyclase/3',5'-cyclic guanosine monophosphate/protein kinase G signaling pathway: an in vitro study. Endocrinology. 2003; 144(7):3114–29. https://doi.org/10.1210/en.2002-0167 ISI:000183547800045. PMID: 12810568

95. Mruk DD, Cheng CY. Sertoli-Sertoli and Sertoli-germ cell interactions and their significance in germ cell movement in the seminiferous epithelium during spermatogenesis. Endocr Rev. 2004; 25(5):747–806. https://doi.org/10.1210/er.2003-0022 ISI:000224281000003. PMID: 15466940

96. Barros JBD, da Silva PAN, Koga RDR, Gonzalez-Dias P, Carmo JR, Nagib PRA, et al. Acute Zika virus infection in an endemic area shows modest proinflammatory systemic immunoactivation and cytokine-symptom sssociations. Front Immunol. 2018; 9. Artn 821 https://doi.org/10.3389/Fimmu.2018.00821 ISI:000431333200001. PMID: 29774022

97. Nishiyama R, Podolsky DK, Reinecker HC. Regulation of tight junction formation in intestinal epithelial cells by the IL-15 ligand-receptor system. Gastroenterology. 1998; 114(4):A898–A. https://doi.org/10.1016/S0016-5085(98)83655-X ISI:000073089603658.

98. Aid M, Abbink P, Larocca RA, Boyd M, Nityanandam R, Nanayakkara O, et al. Zika virus persistence in the central nervous system and lymph nodes of rhesus monkeys. Cell. 2017; 169(4):610–20. https://doi.org/10.1016/j.cell.2017.04.008 ISI:000400560900008. PMID: 28457610

99. Guerriero G, Trocchia S, Abdel-Gawad FK, Ciarcia G. Roles of reactive oxygen species in the spermatogenesis regulation. Front Endocrinol. 2014; 5. Artn 56 https://doi.org/10.3389/Fendo.2014.00056 ISI:000209749800058. PMID: 24795696

100. Regueira M, Riera MF, Galardo MN, Pellizzari EH, Cigorraga SB, Meroni SB. Activation of PPAR alpha and PPAR beta/delta regulates Sertoli cell metabolism. Mol Cell Endocrinol. 2014; 382(1):271–81. https://doi.org/10.1016/j.mce.2013.10.006 ISI:000330421600029. PMID: 24128860

101. Gold L. Unbiased affinity-based proteomics: SOMAscan applications for healthcare. FEBS J. 2013; 280:632–. ISI:000325919203511.

102. Gold L, Ayers D, Bertino J, Bock C, Bock A, Brody EN, et al. Aptamer-based multiplexed proteomic technology for biomarker discovery. PLoS One. 2010; 5(12):e15004. ARTN e15004 https://doi.org/10.1371/journal.pone.0015004 ISI:000285041800017. PMID: 21165148

103. Nickol ME, Ciric J, Falcinelli SD, Chertow DS, Kindrachuk J. Characterization of host and bacterial contributions to lung barrier dysfunction following co-infection with 2009 pandemic influenza and methicillin resistant Staphylococcus aureus. Viruses. 2019; 11(2):116.

104. Coombs KM, Berard A, Xu W, Krokhin O, Meng X, Cortens JP, et al. Quantitative proteomic analyses of influenza virus-infected cultured human lung cells. J Virol. 2010; 84(20):10888–906. Epub 2010/08/13. JVI.00431-10 [pii] https://doi.org/10.1128/JVI.00431-10 PMID: 20702633; PubMed Central PMCID: PMC2950599.